WAVES IN NUMERICAL AND PHYSICAL WAVE FLUMES – A DETERMINISTIC COMBINATION

HAIWEN ZHANG

DHI Water & Environment, Agern Allé 5, DK-2970 Hørsholm, Denmark
Department of Mechanical Engineering, Technical University of Denmark, DK-2800 Kgs. Lyngby, Denmark
(zhw@dhi.dk)

HEMMING A. SCHÄFFER

DHI Water & Environment, Agern Allé 5, DK-2970 Hørsholm, Denmark
(has@dhi.dk)

A deterministic combination of a numerical and a physical model for wave flumes is presented. In the combined model, a Boussinesq model (MIKE 21 BW) is chosen for the numerical calculation. A wave flume with a piston type wavemaker and the Active Wave Absorption Control System (DHI AWACS) is utilized for the physical model. The link between the numerical and physical models is made by an ad hoc unified wave generation theory, which is devised in the paper. This theory accounts for shallow water nonlinearity and compensates for local wave phenomena (evanescent modes) near the wavemaker.

1. Introduction

In coastal engineering, water wave problems are frequently studied by either numerical models or physical models. Both approaches have their strengths and weaknesses. Numerical models are often used for large areas, but they are typically unable to accurately capture highly non-linear physics including wave breaking. Physical models are suitable to simulate complex non-linear processes near the shore or near fixed or floating structures, but they are restricted by the scale and the size of the facility. The limited extent of the physical model often prohibits that the offshore boundary is located in sufficiently deep water for the incident waves to be well described by standard, parameterized wave spectra. As this is typically the only available incident wave description, the limited size of the model facility often precludes important local phenomena like refraction and diffraction. The integrated use of the two approaches could offer an attractive alternative to using either alone. A suitable combination would be a physical model focusing on the complex part of the problem near the shore or near structures and a numerical model for the surrounding wave transformation.

Typically, the combination of numerical and physical models has been to use a numerical model for the determination of the wave conditions at the

boundary of the physical model. In the traditional combined modelling approach, the data transfer between the numerical and the physical model is only on a stochastic level through bulk parameters, such as the significant wave height and spectral peak frequency.

This study aims at a deterministic combination of a numerical model and a physical model for waves in two horizontal dimensions. The present paper only considers the wave flume case. We choose a Boussinesq model (MIKE 21 BW, Madsen and Sørensen, 1992) for the numerical wave computations in the far field. This model has a reasonable balance between accuracy and computational expense. A wavemaker and the associated control system with active absorption provide the interface between the numerical and physical models. The piston-type wavemaker is controlled for simultaneous wave generation and active absorption by the Active Wave Absorption Control System (DHI AWACS). A new heuristic unified wave generation method is devised that accounts for shallow water nonlinearity and compensates for local wave phenomena (evanescent modes) near the wavemaker. This ad hoc unified wave generation provides the link between numerical and physical models for the deterministic combination.

Three different types of wavemaker control are offered by the DHI AWACS. In *position mode*, the control signal is time series of wavemaker paddle position. This mode is compatible with the general approach to nonlinear wave generation. However, active absorption is not included in *position mode*. *Single mode* is a traditional approach for active absorption, in which the control signal is the incident progressive wave elevation. The weakness of *single mode* is inconsistent nonlinear wave generation. A third method termed *dual mode* has been developed recently (Schäffer and Jakobsen, 2003). This allows for consistent nonlinear wave generation in combination with active absorption. The active absorption appears as a linear perturbation on the nonlinear wave generation. The control signals in *dual mode* are time series of wavemaker paddle position and the corresponding surface elevation at the moving paddle. These two control signals are provided by the ad hoc unified wave generation.

2. Ad Hoc Unified Wavemaker Theory for Wave Flumes

This chapter writes up linear wavemaker theory in a suitable form, reviews the equation for nonlinear shallow water wave generation, and shows how the two can be combined in an ad hoc manner.

Time series of surface elevation, depth-averaged horizontal particle velocity at the wave paddle, and paddle position are denoted $\eta(t)$, $U(t)$, and $X(t)$,

respectively, in the time domain, while $A(\omega)$, $B(\omega)$ and $X_a(\omega)$ denote the equivalent complex Fourier amplitudes in frequency domain:

$$\eta(t) \overset{\text{FourierTransform}}{\Leftrightarrow} A(\omega) \ , \tag{1}$$

$$U(t) \overset{\text{FourierTransform}}{\Leftrightarrow} B(\omega) \ , \tag{2}$$

$$X(t) \overset{\text{FourierTransform}}{\Leftrightarrow} X_a(\omega) \ . \tag{3}$$

Here t is time and ω is angular frequency. The quantities A and η carry the following subscripts: "*I*" for the target, progressive, incident waves, "*0*" for waves measured right at the paddle front, and "*I,0*" for the expected wave elevation at the paddle front.

2.1. *Linear Wave Generation*

According to linear fully dispersive wavemaker theory, the paddle position amplitude relates to the progressive wave amplitude as

$$ic_0 X_a(\omega) = A_I(\omega) \ . \tag{4}$$

Here, i is the imaginary unit showing a 90 degree phase shift, and c_0 is known as the Biesel transfer function. For a piston-type wavemaker, we have

$$c_0 = \frac{4\sinh^2 kh}{2kh + \sinh 2kh} \ , \tag{5}$$

where k is the wave number and h is the water depth. With B denoting the complex amplitude of the depth-averaged velocity, mass conservation yields,

$$B(\omega) = \frac{\omega}{kh} A_I(\omega) \ . \tag{6}$$

Eliminating $A_I(\omega)$ from eq.(4) and (6), we get

$$i\omega X_a(\omega) = \Lambda B(\omega) \ , \tag{7}$$

where

$$\Lambda \equiv \frac{kh}{c_0} = \frac{kh(2kh + \sinh 2kh)}{4\sinh^2 kh} \ . \tag{8}$$

Figure 1 shows Λ versus non-dimensional angular frequency $\omega\sqrt{h/g}$. Since the Boussinesq model providing the incident waves is only accurate up to $kh \approx 3$ ($\omega\sqrt{h/g} \approx \sqrt{3}$), we may damp the high-frequency response by replacing Λ with a modified Λ_m as shown in Figure 1a. Both Λ and Λ_m tend to unity when

the frequency tends to 0. Thus the dispersion correction vanishes in the long-wave limit.

Eq. (7) may be rewritten as two equations

$$\begin{aligned} i\omega X_a^{sw}(\omega) &= B(\omega) \qquad \text{(a)} \\ X_a(\omega) &= \Lambda_m X_a^{sw}(\omega) \qquad \text{(b)}\,. \end{aligned} \tag{9}$$

where superscript "*sw*" indicates the use of shallow water theory for obtaining the paddle position from the depth-averaged particle velocity at the mean paddle position. Eq. (9b) gives a dispersion correction by which the shallow water result is turned into a result valid for all relevant water depth.

By the Inverse Fourier Transform and the convolution theorem, the wave paddle position in the time domain can be expressed as

$$\frac{dX^{sw}(t)}{dt} = U(t)\ , \tag{10}$$

$$X(t) = \int_{-t_0}^{t_0} X^{sw}(t-t')\lambda_m(t')dt'. \tag{11}$$

where $\lambda_m(t)$ is the impulse response function corresponding to $\Lambda_m(\omega)$ for the dispersion correction, see Figure 1b. Here t_0 is in principle infinite, but in practice it may be chosen to reflect the effective width of the impulse response function.

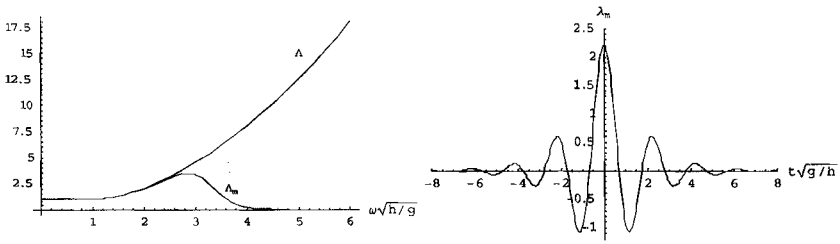

Figure 1. (a) The transfer function for the dispersion correction Λ and the modified transfer function Λ_m versus non-dimensional frequency. (b) Impulse response function for the modified dispersion correction.

For active absorption with *dual mode*, the surface elevation at the moving paddle is furthermore required. Due to the mismatch between the shape of the wave paddle and the vertical profile of the horizontal velocity of progressive waves, an evanescent wave field exists at the paddle front. From linear wavemaker theory, we obtain,

$$A_{I,0}(\omega) = A_I(\omega) + \Gamma X_a(\omega) . \tag{12}$$

where

$$\Gamma \equiv i\sum_{j=1}^{\infty} c_j , \tag{13}$$

and

$$c_j = \frac{4\sinh^2 k_j h}{2k_j h + \sinh 2k_j h} . \tag{14}$$

Here, k_j is purely imaginary corresponding to evanescent modes, and satisfies the linear dispersion relation generalized to complex wave numbers,

$$\omega^2 = gk_j \tanh k_j h . \tag{15}$$

The transfer function Γ is modified to Γ_m by damping at high frequencies as done for Λ, see Figure 2a. Both Γ and Γ_m tend to 0 when the frequency tends to 0. Thus the evanescent-mode correction vanishes in the long-wave limit.

The surface elevation at the moving paddle in the time domain is expressed as

$$\eta_{I,0}(t) = \eta_I(t) + \int_{-t_0}^{t_0} X(t-t')\gamma_m(t')dt' . \tag{16}$$

Here $\gamma_m(t)$ is the impulse response function corresponding to $\Gamma_m(\omega)$, see Figure 2b.

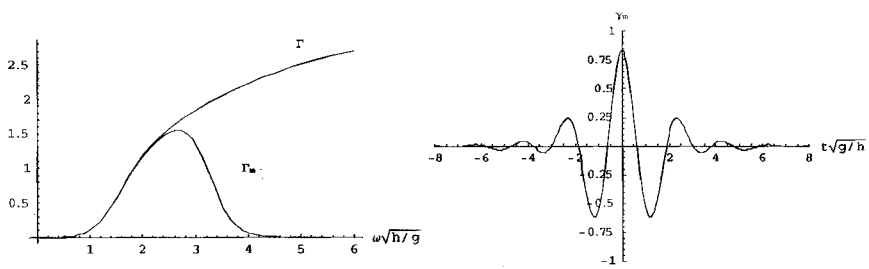

(a) (b)

Figure 2. (a) The transfer function for evanescent-mode correction Γ and the modified transfer function Γ_m versus non-dimensional frequency. (b) Impulse response function for evanescent-mode correction.

2.2. *Nonlinear Shallow Water Wave Generation*

For nonlinear shallow water waves with small dispersion such as Cnoidal waves, the horizontal particle velocity is almost uniform over depth. The time-domain relation between the depth-averaged velocity and the paddle position is given directly as

$$\frac{dX^{sw}(t)}{dt} = U(X^{sw}(t),t) \quad , \tag{17}$$

with the initial condition $X^{sw}(0)=0$. This approach was used successfully by Goring et al. (1978) for Cnoidal waves. This step captures the nonlinearity of the numerical model, but corresponds to the shallow water limit for the wave generation.

For active absorption in *dual mode*, the associated surface elevation at the moving paddle is also needed,

$$\eta_{I,0}(t) = \eta(X^{sw}(t),t) \quad . \tag{18}$$

2.3. *Ad Hoc Unified Wave Generation*

Based on the linear fully dispersive wavemaker theory and the method of nonlinear long-wave generation, we make an ad hoc combination. In order to avoid slow drift of the paddle, a small term proportional to the paddle signal is added to the differential equation. This has the effect of a first order high-pass filter. Let ω_c denote the characteristic angular frequency of this filter, then the unified wave generation is altogether governed by

$$\frac{dX^{sw}(t)}{dt} + \omega_c X^{sw}(t) = U(X^{sw}(t),t) \, , \tag{19}$$

followed by the dispersion correction

$$X(t) = \int_{-t_0}^{t_0} X^{sw}(t-t')\lambda_m(t')dt' \, . \tag{20}$$

For *dual mode* active absorption, the expected surface elevation at the moving paddle $\eta_{I,0}(t)$ with evanescent-mode modification is also needed. We have

$$\eta_{I,0}(t) = \eta(X(t),t) + \int_{-t_0}^{t_0} X(t-t')\gamma_m(t')dt' \quad . \tag{21}$$

For long waves (where the evanescent modes disappear), this method is consistent with nonlinear long-wave generation. For small amplitude waves, the fully dispersive wavemaker theory is recovered.

3. Tests of the Combined Model with Deterministic Combination

In the combined model, the MIKE 21 BW 2D module is chosen for the numerical model. As an extension of the numerical flume, physical tests are

made in a 0.75m wide, 1.20m deep and 23m long flume. The ad hoc unified wave generation is applied as the link between the numerical and the physical model. The flume is equipped with a piston-type wavemaker with an electric drive system including a brushless AC motor and an integrated linear drive/ bearing system. The wavemaker is controlled by the DHI AWACS with three different control modes. Several tests of the combined model are presented below. In all tests, the numerical model is run beyond the wavemaker to provide a reference for the wave elevations time series measured in the physical experiment.

3.1. *Nonlinear Shallow Water Wave Cases*

The combined model is run with Cnoidal wave input to the numerical model. The wave period is T=2.3s, and the wave height is H=0.12m. Throughout the numerical and physical wave flumes, the water depth is constant, h=0.4m. This gives kh=0.56 and an Ursell number, Ur=37.6. For the numerical simulation, the grid spacing is taken as dx=0.1m and the time step is dt=0.01s. The control signals required for the physical test are calculated by the unified wave generation method. For each numerical model execution, three different physical model tests were made each with a different control mode for the wave generation/active absorption system. These three modes (*single mode*, *dual mode* and *position mode*) were described in the introduction. Two wave gauges are set at 1.0m and 4.4m from the mean paddle in the physical flume. The wave surface elevation measured at these gauges are compared with the numerical calculation, see Figure 3.

The measurements in *dual mode* and *position mode* match the numerical results reasonably well. The result for *single mode* is less good, which is expected due to the inconsistent nonlinear wave generation. *Single mode* will not be discussed in the following.

We now test the combined model for Cnoidal waves with higher non-linearity by increasing wave height to H=0.20m with the same period T=2.3s and depth h=0.4s. For this case, we have kh=0.53 and Ur=70.8. The wave surface elevation measured at the two gauges is compared with the numerical calculation in Figure 4. We notice that at the gauge 4.4m both *dual mode* and *position mode* give higher elevation peaks than expected by the numerical result. To investigate the reason for this mismatch, we first eliminate the numerical model by testing waves with the same conditions (T=2.3s, h=0.4m, H=0.20m) but generated by Cnoidal wavemaker theory in the physical flume. The measurements of surface elevation are compared with the theoretical Cnoidal waves in Figure 5. The same phenomenon happens as before, the peaks of the surface elevation measured in *dual mode* and *position mode* are still much

higher than the theoretical elevation at the gauge 4.4m from the mean paddle. This shows that Cnoidal (wavemaker) theory is inadequate for highly nonlinear waves. Also Figures 4 and 5 are quite similar indicating that possible errors in the numerical wave flume (the Boussinesq model) have little effect in this case.

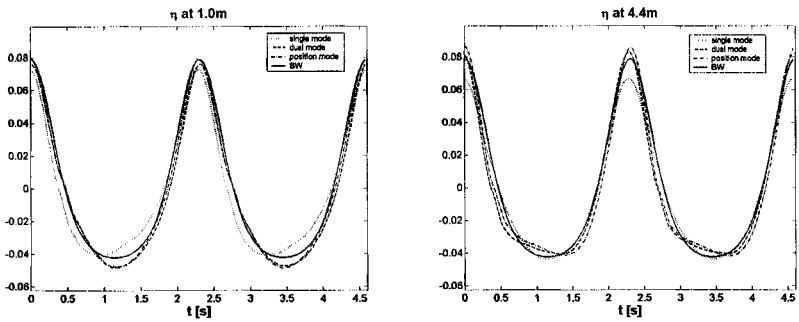

Figure 3. Wave surface elevation measured at two gauges for H=0.12m compared with the numerical calculation (BW). Results are shown for three different control modes.

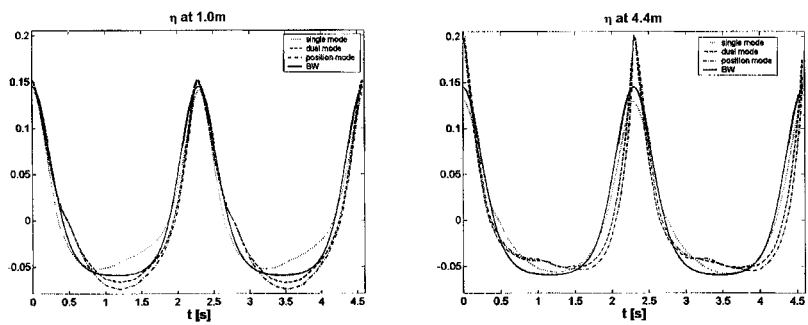

Figure 4. As Figure 3, but for H=0.20m.

To further investigate the reason for the difficulty in obtaining these quite nonlinear waves of constant form in the physical wave flume, we turn to Stream function theory (Dean, 1965). Thus waves are generated according to Section 2.2, but using Stream Function wave theory to represent the depth-averaged velocity. For T=2.3s, h=0.4m, and H=0.20m the measurements of surface elevation are compared with the solution of the Stream function theory wave in Figure 6.

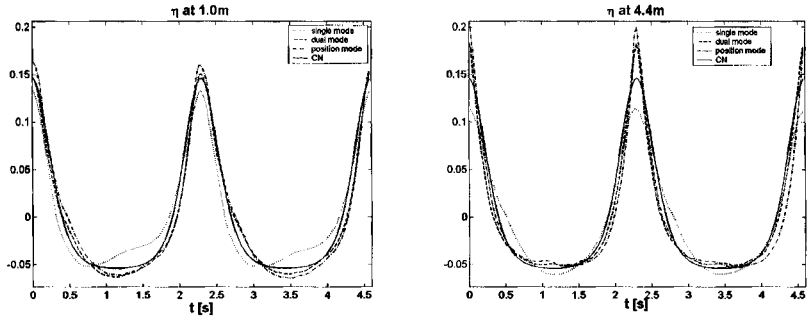

Figure 5. The measurements of waves generated by Cnoidal wavemaker theory for H=0.20m compared with the theoretical solution (CN).

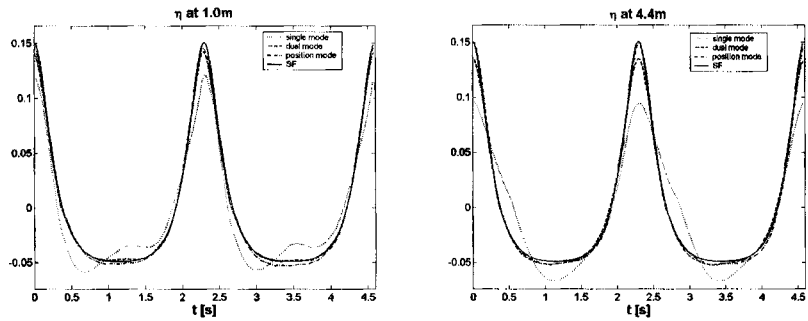

Figure 6. The measurements of waves generated by the "Stream Function wavemaker theory" for H=0.20m compared with the theoretical solution (SF).

The measurements of surface elevation in *dual mode* and *position mode* now match the theoretical solution very well at each gauge. Especially, at the gauge at 4.4m, the results are improved a lot comparing with the results by Cnoidal wavemaker theory. Thus for this shallow case, the surface elevation of highly nonlinear waves is reproduced very well by the "Stream Function wavemaker theory". In conclusion, the problem of the combined numerical and physical model (see Figure 3) lies in the limited accuracy of the numerical model and its up-wave boundary conditions, and not in the procedure for obtaining the wavemaker control signals or in the physical model.

3.2. *Irregular Waves Propagating on Constant Water Depth*

With the purpose of testing the dispersion correction and the evanescent-mode correction, we now turn to a rather deepwater case for irregular waves.

As *dual mode* is the only control mode that can handle nonlinear wave generation and active absorption simultaneously, only results for this method will be shown in the remaining part of the paper.

The simulated wave flume is 160m long with a constant water depth of h=0.7m. The irregular incoming wave conditions are synthesized from a standard JONSWAP frequency spectrum, with a significant wave height of H_{m0}=0.05m, a peak period of T_p=1.2s, and the relevant shape parameters, γ=3.3, σ_a=0.07, σ_b= 0.09. The spectrum is truncated omitting periods smaller than 0.95s. This gives a range of kh between 2.02 and 3.13. The truncated spectrum is re-scaled in the numerical model to retain the specified H_{m0}=0.05m. The time step is taken as dt=0.01s and the grid spacing is dx=0.1m. We set fixed wave gauges at x=100m and x=103.4m, where x=0 coincides with the up-wave boundary of the numerical model. For the data transfer between the numerical and physical models, we choose to test two different locations, x_0=96m and x_0=99m. Thus x_0 is the mean paddle position for the physical flume.

The surface elevations measured at 4.0m and 7.4m from the mean paddle position in the physical flume are compared with the numerical calculations when choosing x_0=96m in Figure 7. The correlation coefficients are 0.987 at gauge 1 and 0.968 at gauge 2 in the whole 10-min period of the physical tests. The comparison of the surface elevations measured at 1.0m and 4.4m from the mean paddle in the physical flume with the numerical calculations is shown in Figure 8 for the case of x_0=99m. Note that the gauge positions were chosen to leave the distance to the up-wave boundary of the numerical model unchanged. Thus, the target (BW) in Figures 7 and 8 are identical. The correlation coefficients between measured and numerical surface elevation are 0.994 at gauge 1 and 0.985 at gauge 2 for the 10-min duration of physical test. All the measurements in physical flume match the numerical calculation well. The measurement is closer to the numerical result when the wave gauge is closer to the mean paddle position. This is due to the limited accuracy of the numerical model. However, the combined model is almost independent of the mean paddle's location. Therefore, the combined model is not sensitive to where the physical model takes over from the numerical model.

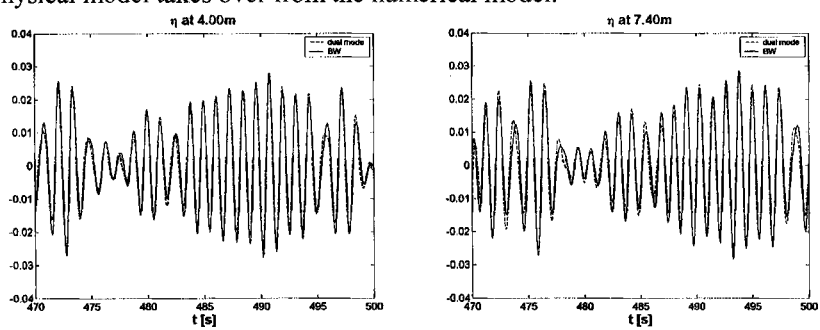

Figure 7. The surface elevation measured at 4.0m and 7.4m (using *dual mode* control) compared with the numerical calculation (BW) choosing $x0$=96m.

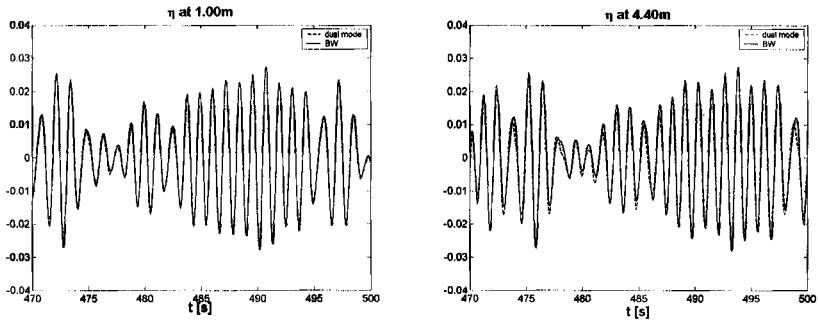

Figure 8. The surface elevation measured at 1.0m and 4.4m (using *dual mode* control) compared with the numerical calculation (BW) choosing $x0$=99m. Altogether, this gives a target (BW) which is identical to that of Figure 7.

3.3. *Irregular Waves Propagating up a Slope*

The last example considers irregular waves propagating up a slope from a deep plateau to a shallow plateau. At the end of the slope, the nonlinearity is very high. The length of the simulated wave flume is 160m. The internal wave generation of the numerical model is set at x=10.2m with the deepwater depth of 2.6m. The slope is 1/50 and the shallow water depth is 0.4m. The irregular incident wave conditions were synthesized from a standard JONSWAP frequency spectrum, with a significant wave height of H_{m0}=0.12m, a peak period of T_p=3s, and the relevant shape parameters, γ=3.3, σ_a=0.07, σ_b= 0.09. The spectrum is truncated omitting periods smaller than 2.6s. The time step is taken as dt=0.01s and the grid spacing is dx=0.1m. As an example, Figure 9 shows profiles of depth-integrated velocity (P flux) and surface elevation at t=180s extracted from the numerical output at the part of the flume with constant shallow water depth. After shoaling, the waves have turned into irregular nonlinear long waves. The physical model is set at the flat shallow water depth, h=0.4m. We set two fixed wave gauges at x=128.2m and x=131.6m in the entire simulated flume. For the data transfer between numerical and physical models, we choose two locations x_0=125.2m and x_0=127.2m as the mean paddle positions for the physical flume tests.

The surface elevations measured at 3.0m and 6.4m from the mean paddle in the physical flume are compared with the numerical calculations in Figure 10 choosing x_0=125.2m. The correlation coefficients are 0.947 at gauge 1 and 0.941 at gauge 2 for the entire 10-min duration. Although deviations occur especially for the higher waves, the match is quite good considering the very high non-linearity of the waves. The Ursell number is about 71 at significant wave height and peak period, and thus about twice that of the highest waves in the wave train. In fact, some wave breaking occurred in the physical flume on the down-

wave side of the wave gauges. Wave breaking was not accounted for in the numerical model.

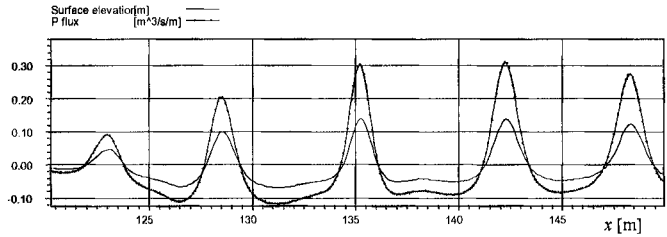

Figure 9. Profiles of depth-integrated velocity (P flux) and surface elevation at constant water depth h=0.4m at t=180s.

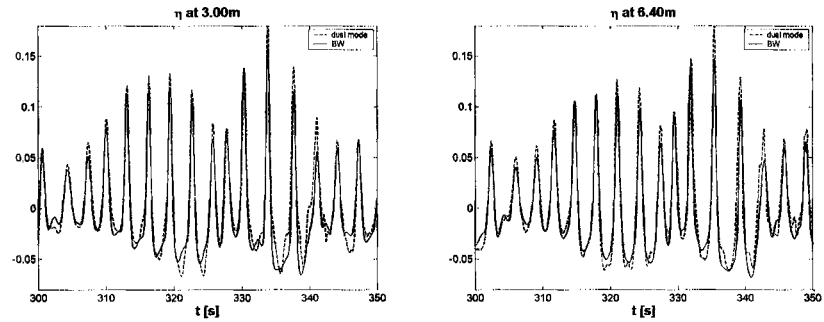

Figure 10. The surface elevation measured at 3.0m and 6.4m (using *dual mode* control) compared with the numerical calculation (BW) choosing x_0=125.2m.

We now repeat the test but with the mean paddle position shifted 2m to x_0=127.2m. The two wave gauges are moved accordingly in order to measure elevation time series at the same distance from the up-wave boundary of the numerical flume as before. The comparison of the surface elevations measured at 1.0m and 4.4m from the mean paddle in the physical flume with the numerical calculations is shown in Figure 11 for the case of x_0=127.2m. The correlation coefficients are 0.942 at gauge 1 and 0.948 at gauge 2 for the entire duration.

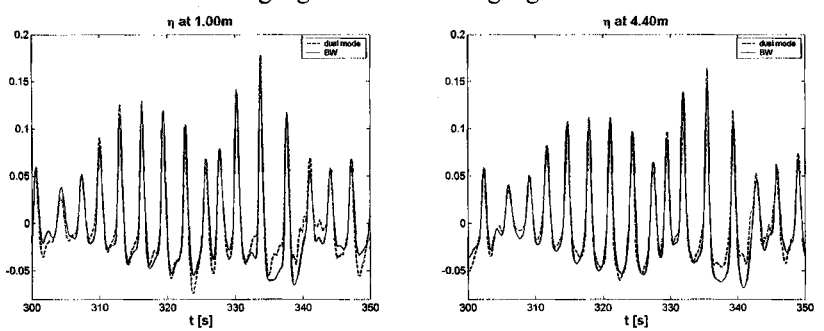

Figure 11. The surface elevation measured at 1.0m and 4.4m (using *dual mode* control) compared with the numerical calculation (BW) choosing x_0=127.2m. Altogether, this gives a target (BW) which is identical to that of Figure 10.

4. Summary and Conclusions

In this paper, an ad hoc unified wave generation theory for wave flumes has been devised that accounts for shallow water nonlinearity and local wave phenomena (evanescent modes) near the wavemaker. This theory is shown to be suitable for a deterministic combination of numerical and physical wave flumes.

In general, the combined numerical/physical wave flume tests show that the unified wave generation method is adequate for successfully passing waves from a numerical model to a physical wave flume. Limited accuracy for highly non-linear waves appears to be due to the numerical model rather than to the unified wave generation theory.

This conclusion was supported by the observation that while Cnoidal wavemaker theory was inadequate for highly nonlinear waves, the same wave generation procedures, but using Stream Function theory, significantly improved the results.

Acknowledgments

This work is funded by the Danish Technical Research Council (STVF Contract No 26-01-0043). Kim P. Jakobsen is acknowledged for his help with the physical model tests and his work on the DHI Wave Synthesizer Software to allow custom signals for dual control. Harry B. Bingham is thanked for providing his Mathematica notebook of Stream Function theory.

References

Dean, R.G, 1965. Stream function representation of non-linear ocean waves. Journal of Geophysical Research, 70(18), 4561-4572.

Gierlevsen, T., et al., 2003. Numerical and physical modelling of storm waves at Rio de Janeiro yacht club. COPEDEC VI, Colombo, Sri Lanka, 15-19 Sept. 2003.

Goring, D.G., 1978. Tsunamis - the propagation of long waves onto a shelf. PhD Thesis, Report No. KH-R-38, Cal. Inst. Tech.

Madsen, P.A. and Sørensen, O.R., 1992. A new form of the Boussinesq equations with improved linear dispersion characteristics. Part 2. A slowly-varying bathymetry. Coastal Engineering. Vol.18. 183-204.

Schäffer, H.A. and Jakobsen K.P., 2003. Nonlinear wave generation and active absorption in wave flumes. Long Waves Symposium, Thessaloniki, Greece.
In parallel with XXX IAHR Congress.